Acta Crystallographica Section D
Biological Crystallography
ISSN 0907-4449

Radiation-damage-induced phasing with anomalous scattering: substructure solution and phasing

Petrus H. Zwart,[a] Sankaran Banumathi,[b] Miroslawa Dauter[a] and Zbigniew Dauter[b]*

[a]SAIC-Frederick Inc., Basic Research Program, Brookhaven National Laboratory, Upton, NY 11973, USA, and [b]Synchotron Radiation Reseach Section, MCL, National Cancer Institute, Brookhaven National Laboratory, Upton NY 11973, USA

Correspondence e-mail: dauter@bnl.gov

Received 10 June 2004
Accepted 3 September 2004

Substructure-solution and phasing procedures using a combination of anomalous scattering and radiation-damage-induced isomorphous differences have been investigated. The tyrosine residues in thaumatin were iodinated with *N*-iodosuccinimide in the crystalline form as well as prior to crystallization. Several data sets were collected from both forms and used for substructure solution and phasing using various protocols, employing anomalous, isomorphous or both these signals. It was shown that combination of the anomalous and isomorphous signals in the form of the RIPAS (radiation-damage-induced phasing with anomalous scattering) strategy is beneficial for both locating the substructure and subsequent phasing.

1. Introduction

Structural changes induced by radiation damage have been shown to aid in the phasing process (Evans *et al.*, 2003; Weiss *et al.*, 2004) or can even be the sole source of information in both the substructure-solution and subsequent phasing procedures (Ravelli *et al.*, 2003; Banumathi *et al.*, 2004). Phasing macromolecular X-ray data by exploitation of the site-specific effects of radiation damage can be carried out by splitting up a high-redundancy data set into smaller parts and using the resulting isomorphous differences for phasing. A similar strategy is adopted for the location of the substructure using radiation-damage-induced phasing (RIP) methods: the isomorphous differences between data sets can be used in a traditional SIR fashion to obtain the positions of the substructure *via* direct or Patterson methods.

The radiation damage can be inflicted on the crystal either *via* an elongated 'burning' period between the collection of two data sets or by the collection of a large amount of data from the same crystal. The benefit of the latter method is that the structural changes are followed over the course of time, resulting in a large amount of derivative information instead of only two data sets. Furthermore, this approach facilitates a more appropriate correction for radiation damage in order to boost the anomalous signal, as described by Diederichs *et al.* (2003).

The reported applications of radiation damage in phasing have been based on the site-specific effects on sulfurs in disulfide bridges (Ravelli *et al.*, 2003; Banumathi *et al.*, 2004; Weiss *et al.*, 2004), triiodides (Evans *et al.*, 2003) and brominated uridine (Ravelli *et al.*, 2003; Schiltz *et al.*, 2004). The radiolytic debromination of substituted nucleic acids and the problems it can cause in MAD phasing have been described previously by Ennifar *et al.* (2002); this dehalogenation is a well known photochemical reaction that can be carried out on similar systems such as iodinated tyrosines. Tyrosines can be

Table 1
Results of data collection and processing.

Values in parentheses are for the highest resolution bin (HR; 2.59–2.50 Å for CS and 2.07–2.00 Å for IC). Unit-cell parameters, Wilson plot B values, merging R values, overall and high resolution $\langle I\rangle/\langle\sigma(I)\rangle$ values and χ^2 after merging Friedel pairs in the lowest resolution bin (LR; 30.0–5.38 Å for CS and 30–4.31 Å for IC) are given for each data set for both crystals. f' and f'' are the values refined by *XPREP*. See text for details.

	Crystallized and soaked (CS)				Iodinated and crystallized (IC)			
Space group	$P4_12_12$				$P4_12_12$			
Resolution (Å)	30–2.5				30–2.0			
Mosaicity (°)	1.1				0.28			
	Friedels unmerged		Friedels merged		Friedels unmerged		Friedels merged	
Completeness (%)	96.8 (77.8)		97.5 (83.9)		96.5 (93.9)		95.7 (93.4)	
Redundancy	2.3 (1.5)		4.1 (2.6)		3.8 (3.4)		7.0 (6.5)	
Unique reflections	16095 (1300)		9105 (758)		31746 (3095)		17296 (1643)	
Data set	1	2	3	4	1	2	3	4
Unit-cell parameters								
$a = b$ (Å)	57.16	57.23	57.30	57.35	57.64	57.72	57.82	57.85
c (Å)	151.06	151.26	151.46	151.61	151.28	151.44	151.64	151.66
$B_{\rm Wil}$ (Å^2)	46	46	47	50	22	24	26	28
$R_{\rm merge}$ (overall)	0.056	0.050	0.050	0.052	0.059	0.058	0.060	0.072
$R_{\rm merge}$ (HR)	0.226	0.209	0.262	0.285	0.301	0.341	0.469	0.809
$\langle I\rangle/\langle\sigma(I)\rangle$ (overall)	15.5	18.2	18.3	17.6	20.1	22.8	21.5	18.6
$\langle I\rangle/\langle\sigma(I)\rangle$ (HR)	2.4	2.8	2.3	1.9	4.0	3.7	2.6	1.4
χ^2/χ^2 (LR)	3.9/1.0	3.7/1.0	3.7/1.0	3.1/1.0	1.9/1.0	1.8/1.1	1.5/1.0	1.7/1.1
f'/f''	−0.8/9.5	−0.6/7.7	−0.5/6.6	−0.4/5.8	−0.7/6.5	−0.6/5.8	−0.5/5.3	−0.4/8.0

iodinated by treating the protein with *N*-iodosuccinamide (Brzozowski *et al.*, 1991; Leinala *et al.*, 2002) or by soaking protein crystals for an extended time in a triiodide solution (Kretzinger, 1968; Sigler, 1970). The iodination of tyrosine is an electrophilic aromatic substitution on the hydroxyl-activated *ortho* carbon positions and results in either mono- or di-substituted iodotyrosine.

Iodine gives a significant amount of anomalous signal at wavelengths easily reachable at most synchrotron beamlines and at home sources, making it a potent derivatization agent. Furthermore, the anomalous signal in combination with possible isomorphous differences obtained *via* radiation damage allows the SAD and SIR inherent phase ambiguity to be broken, enhancing the quality of experimental electron-density maps, in analogy to the MAD and SIRAS method. Because this phasing strategy is closely related to the RIP method as proposed by Ravelli & McSweeney (2000) but includes anomalous scattering as well, we propose the acronym RIPAS (radiation-damage-induced phasing with anomalous scattering) for this type of phasing scenario.

2. Methods

2.1. Protein crystallization and derivatization

The 207-residue protein thaumatin was crystallized by the hanging-drop method using a protein solution of approximately 30 mg ml^{-1}, 0.8 *M* sodium/potassium tartrate and a 0.1 *M* sodium *N*-(2-acetoamido)iminodiacetic acid (ADA) buffer pH 6.5 (Ko *et al.*, 1994). These native crystals were subsequently soaked for approximately 20 min in mother liquor 25% saturated with *N*-iodosuccinamide. A similar derivative was prepared by iodinating thaumatin prior to crystallization using the same reagent. Crystals suitable for X-ray diffraction grew from conditions similar to those used for native thaumatin.

Four X-ray data sets were obtained from a thaumatin crystal soaked in a diluted *N*-iodisuccinamide solution (hereafter denoted CS) and from iodinated and subsequently crystallized thaumatin (hereafter denoted IC). Data were collected using a wavelength of 1.54 Å and at a temperature of 100 K at the NSLS beamline X9B (Brookhaven National Laboratory). The program *BEST* (Popov & Bourenkov, 2003) was used to aid the decision-making process during data collection. All data sets from both crystals were measured consecutively without any 'burns' in between. The data were integrated and scaled with *HKL*2000 (Otwinowski & Minor, 1997).

2.2. Substructure solution, phasing and structure refinement

XPREP (Sheldrick, 2001) was used to extract anomalous and isomorphous differences. Pseudo-$F_{\rm A}$ values were constructed, treating the subsequently measured data sets as a MAD experiment. Substructure solutions were generated by *SHELXD* (Schneider & Sheldrick, 2002) using either the anomalous or the isomorphous differences as well as the pseudo-$F_{\rm A}$ values. The programs *SITCOM* (Dall'Antonia *et al.*, 2003) and *EMMA* (Grosse-Kunstleve & Adams, 2003) were used for the interpretation of the substructure solutions.

Phasing was carried out with *SHARP* (de La Fortelle & Bricogne, 1997) using a typical SAD or SIR hierarchical set-up. The isomorphous and anomalous differences were simultaneously used in a 'RIPAS' set-up, as proposed by Evans *et al.* (2003). The RIPAS phasing was carried out using the first and second data set, as well as using all four data sets together. Density modification was carried out with *SOLOMON* (Abrahams & Leslie, 1996). Model rebuilding was performed using *XtalView* (McRee, 1999). The protein structure was refined with *REFMAC*5 (Murshudov *et al.*, 1999; Collaborative Computational Project, Number 4, 1994) and the solvent model was built with *ARP*/*wARP* (Lamzin & Wilson, 1993).

3. Results and discussion

3.1. Data acquisition

The CS thaumatin crystal soaked in *N*-iodosuccinimide diffracted to approximately 2.5 Å. The four data sets collected from this crystal covered the same 60° with a $\Delta\varphi$ equal to 1.0° and 60 s exposure per image. According to *RADDOSE* (Murray *et al.*, 2004), this corresponds to about 7.6×10^5 Gy per individual data set. The crystal was mounted in such a way that the *c* axis was approximately 17° away from the spindle direction in order to minimize overlaps resulting from this long axis. The final completeness was 97.5% and the overall redundancy was 4.1. When considering two Friedel mates to be independent reflections, the so-called anomalous redundancy and anomalous completeness were 2.3 and 96.8%, respectively.

The IC crystal of thaumatin iodinated prior to crystallization diffracted to about 2.0 Å. A total of four data sets were collected covering the same 90° with 60 s exposures of 0.5° width, resulting in about 2.5×10^6 Gy per data set. As was the case for the previous crystal, the long axis was mounted at a small angle to the spindle axis (25°) in order to minimize overlaps during data acquisition. The completeness and redundancy were 95.7% and 7.0, respectively. The anomalous completeness and the redundancy were 96.5% and 3.8, respectively. Wilson plot *B* values for all data sets were estimated with *ARP*/*wARP* (Morris *et al.*, 2004). Detailed data-collection statistics for both crystals are shown in Table 1.

Evidence of radiation damage during data collection was obvious from the change in unit-cell parameters from data set to data set, as well as from the loss of diffracting power (Table 1). Other evidence of radiation damage even within the first data sets of both crystals was obtained from a plot of χ^2 as a function of image number provided by *SCALEPACK*, which showed a convex behavior (Fig. 1). This typical behavior of χ^2 as a function of the image number is a characteristic sign of radiation damage (Otwinowski, 2003). This effect can be explained by the fact that the reflections collected halfway through the experiment have intensities that are more similar to overall merged values. The reflections measured at the beginning and the end of the experiment differ most from their averaged intensity.

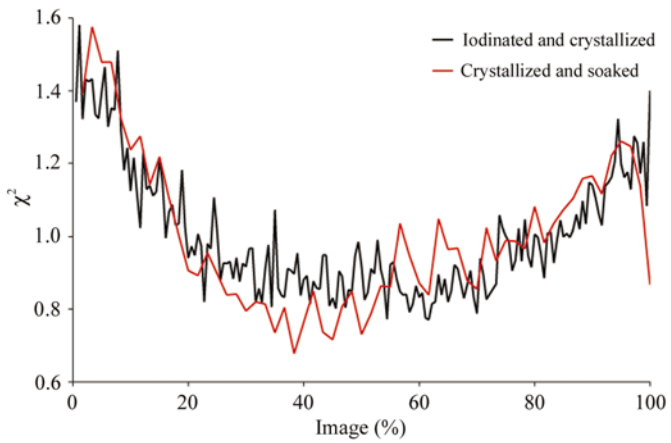

Figure 1
χ^2 as a function of the frame position in the first data set for CS thaumatin (red line) and IC thaumatin (black line).

3.2. Structure refinement and iodinated tyrosine residues

Refinement and remodelling of the structure, including the protein and the ordered solvent molecules, against data sets CS1 and IC1 was carried out with *ARP*/*wARP* in order to obtain model phases for validation of substructure-solution and phasing results. The starting model was the thaumatin structure obtained previously (Banumathi *et al.*, 2004). Refinement against the first CS data set resulted in a model with an *R* and $R_{\rm free}$ of 0.23 and 0.28, respectively. Analogous refinement against the first IC data set resulted in an *R* and $R_{\rm free}$ of 0.18 and 0.23, respectively.

Six iodine sites were located in the IC structure on the basis of an anomalous difference map, whereas nine iodine sites were present in the CS structure. Thaumatin contains a total of eight tyrosine residues. Five of the most solvent-accessible tyrosines are iodinated in the CS structure (doubly substituted Tyr11, Tyr57, Tyr95 and Tyr99 and singly substituted Tyr169). The three tyrosine residues that are not iodinated (Tyr157, Tyr183 and Tyr199) are less solvent-accessible. The IC structure has four iodinated tyrosines (Tyr57 and Tyr95 doubly substituted and Tyr157 and Tyr169 singly substituted). No double conformations of iodinated tyrosine residues were observed in the IC structure, whereas two tyrosine residues in the CS structure have multiple conformations (Tyr11 and Tyr99). Fig. 2 shows the $2F_{\rm o} - F_{\rm c}$ electron density and the anomalous difference map of the first IC data set around the doubly iodinated Tyr95. The isomorphous difference map between the first two IC data sets is also shown.

The occupancies of the iodine sites were refined with *MLPHARE* (Otwinowski, 1991) according to a procedure suggested by Dodson (2003) in which the calculated structure-factor amplitudes of the protein model without the I atoms are treated as native data and the measured amplitudes are treated as derivative data. The resulting occupancies lie

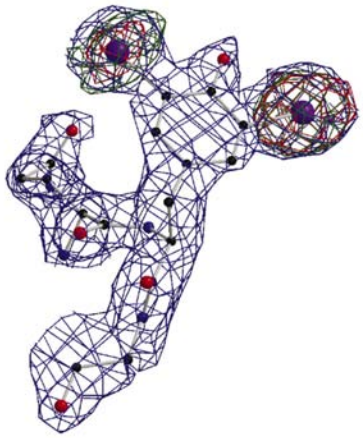

Figure 2
Anomalous (red) and isomorphous (green) difference maps at the 5σ level around iodinated tyrosine Tyr95 in the IC thaumatin structure. The $2F_{\rm o} - F_{\rm c}$ density is shown at a level of 1σ in blue.

between 0.7 and 0.1 for the first CS data set and between 0.6 and 0.2 for the first IC data set.

3.3. Substructure solution

The correlation coefficients of the anomalous differences between the first and second measured data set have values of larger than 50% to 2.7 Å resolution for the CS data and to 2.6 Å for the IC data. Solving the substructure with *SHELXD* using only the Bijvoet differences of the first data set for both crystals has been carried out using the parameters specified in Table 2. The root-mean-square deviation (r.m.s.d.) of the positional parameters of the sites in the best solution from the coordinates of the iodines in the final model are given in Table 2. The *SHELXD* success rate, *i.e.* the number of solutions obtained by *SHELXD* that have more than 50% of atoms within 2 Å of the correct substructure out of 100 trials, is also given to indicate the ease of the substructure-solution process. A similar process was repeated for the substructure solution using only the isomorphous differences (RIP) between data sets 1 and 2. In order to use the anomalous and isomorphous signals at the same time in the substructure solution, the first four data sets from a given crystal have been treated as a MAD system. f' and f'' values were refined in *XPREP* to model the decreasing occupancy of the substructure atoms throughout the subsequent data sets (Table 1). It can be noted that this approach makes no physical sense, as the wavelength is fixed and no changes in f' and f'' are expected. The decrease in occupancy does, however, result in a decrease in the scattering contribution of the (anomalous) substructure, as discussed by Banumathi *et al.* (2004). This effect is different from what one would expect from changes in f' and f''. Treatment of the RIPAS data as if it came from a MAD experiment is thus an approximation.

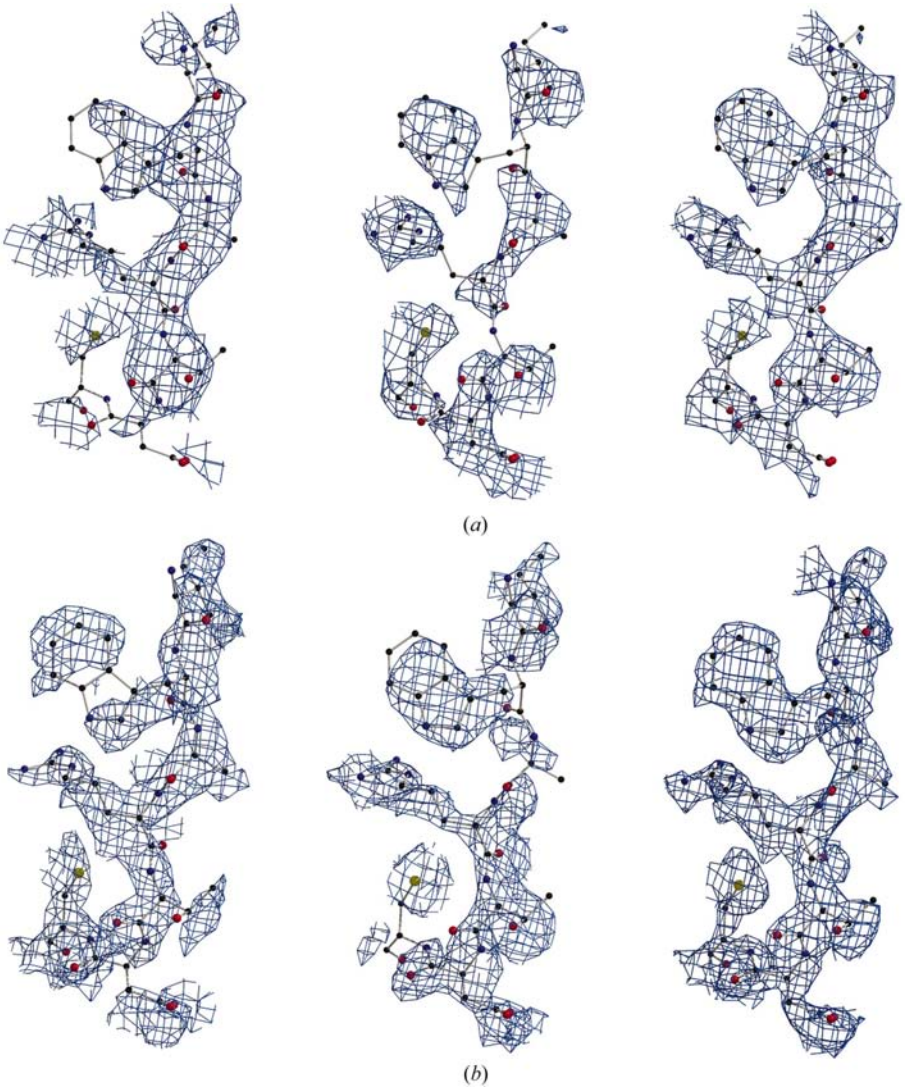

Figure 3
(*a*) Experimental electron density before solvent flattening with SAD (left), RIP (middle) and RIPAS12 (right) phases for the CS thaumatin data. All contour levels are at 1σ. (*b*) Experimental electron density before solvent flattening with the SAD (left), RIP (middle) and RIPAS12 (right) phases for IC thaumatin data. All contour levels are at 1σ.

It can be seen from Table 2 that locating the substructure using either the anomalous or isomorphous differences is successful for both crystals. Using both the anomalous and isomorphous signals to estimate F_A values results in an 88% success rate for the IC data, whereas the SAD and RIP ΔF values resulted in a 70 and 59% success rate, respectively. The CS data did not show this remarkable improvement in performance of *SHELXD* compared with the SAD and RIP protocols, most likely because of the relatively low quality of the data.

Obtaining F_A values from only two data sets was unsuccessful because of the inability to refine the f' and f'' values with a limited amount of data.

3.4. Phasing

The results of the heavy-atom refinement and phasing are given in Table 2. Whereas both the SAD and RIP protocols for both crystals result in phases suitable for a successful run of density modification, the RIPAS phasing using only the first and second data set (RIPAS12) resulted in interpretable electron-density maps even before density modification (Figs. 3*a* and 3*b*). However, the RIPAS phasing protocol using four data sets at once was less successful. Figures of merit and

Table 2
Substructure-solution and phasing results.

SHEL, resolution limits used in *SHELXD*. ESEL/NREF, minimum *E*-value criterion in *SHELXD* and resulting number of selected reflections. *SHELXD* CC, correlation coefficient for all and weak reflections of the best solution. PATFOM, Patterson figure of merit. Correct/r.m.s.d., number of correct substructure sites and the r.m.s.d. of the positional parameters to the final model. *SHELXD* success rate, see text. *SHARP* phasing power (iso a, iso c, ano a), phasing powers for isomorphous acentric, isomorphous centric and anomalous acentric differences. *SHARP* FOM (a, c), figure of merit for acentric and centric reflections. mcc/$\Delta\varphi$ *SHARP*, map correlation and root-mean-square phase difference after *SHARP* to final phases. mcc/$\Delta\varphi$ *SOLOMON*, map correlation and root-mean-square phase difference after *SHARP* and *SOLOMON* to final phases.

(*a*) Crystallized and soaked (CS).

Protocol	SAD	RIP	RIPAS12	RIPAS1234
SHEL (Å)	30.0–3.0	30.0–3.5	See text	30.0–3.5
ESEL/NREF	1.4/708	1.0/1142	See text	1.0/1282
SHELXD CC	38/18	40/9.7	See text	45/20
PATFOM	2.16	4.73	See text	3.42
Correct/r.m.s.d. (Å)	11/0.39	10/0.55	See text	11/0.45
SHELXD success rate (%)	3	21	See text	17
SHARP phasing power (iso a, iso c, ano a)	(0, 0, 1.6)	(0, 0, 0), (1.6, 1.2, 0)	(0, 0, 2.1), (1.6, 1.3, 1.9)	(0, 0, 1.6), (5.2, 3.3, 1.3), (6.9, 4.1, 0.9), (5.8, 3.3, 0.7)
SHARP FOM (a, c)	0.31, 0.15	0.30, 0.43	0.54, 0.45	0.76, 0.71
mcc/$\Delta\varphi$ *SHARP* (°)	0.37/78	0.50/69	0.54/66	0.49/67
mcc/$\Delta\varphi$ *SOLOMON* (°)	0.77/52	0.84/49	0.88/42	0.73/53

(*b*) Iodinated and crystallized (IC).

Protocol	SAD	RIP	RIPAS12	RIPAS1234
SHEL (Å)	30.0–3.0	30.0–3.0	See text	30.0–3.0
ESEL/NREF	1.4/733	1.4/932	See text	1.3/1092
SHELXD CC	48/24	40/20	See text	47/30
PATFOM	8.83	10.64	See text	9.3
Correct/r.m.s.d. (Å)	6/0.22	6/0.34	See text	6/0.22
SHELXD success rate (%)	70	59	See text	88
SHARP phasing power (iso a, iso c, ano a)	(0, 0, 1.3)	(0, 0, 0), (1.3, 1.0, 0)	(0, 0, 1.5), (1.2, 1.0, 1.2)	(0, 0, 1.4), (3.7, 2.3, 0.94), (3.9, 2.5, 0.6), (3.2, 2.1, 0.4)
SHARP FOM (a, c)	0.37, 0.14	0.28, 0.40	0.59, 0.40	0.71, 0.72
mcc/$\Delta\varphi$ *SHARP* (°)	0.49/73	0.47/70	0.65/61	0.57/61
mcc/$\Delta\varphi$ *SOLOMON* (°)	0.93/33	0.91/35	0.94/30	0.81/45

corresponding phasing power were overestimated, possibly owing to the presence of correlated non-isomorphism between data sets (Table 2).

A major benefit of the RIPAS phasing strategy over traditional SAD or SIR-like RIP phasing is that the presence of both the isomorphous and anomalous differences results, at least ideally, in the breakage of the phase ambiguity inherent in SAD and RIP. The fact that the electron densities of the SAD and RIP maps are reasonable can be attributed to the Sim contribution of the relatively large iodine substructure.

4. Conclusions

Although SAD and RIP phasing was successful in the cases presented, the additional information provided by the RIPAS approach not only strengthened the substructure-solution procedure in *SHELXD*, but also produced high-quality experimental electron-density maps. RIPAS thus seems to be a powerful addition to the SAD method when a significant amount of site-specific radiation damage is present in the anomalous substructure. The site-specific radiation damage that might be inflicted on the substructure could obstruct the standard MAD phasing procedure if these effects are not taken into account properly.

The iodinated tyrosine residues obtained in the described experiments are shown to be a powerful source of phasing information, through structural changes generated *via* radiation damage, even on a relatively weak second-generation synchrotron beamline. Furthermore, even a small amount of radiation damage can be successfully utilized for phasing, as evidenced by the successful use of only the first two data sets for the CS and IC crystals. The presence of correlated non-isomorphism seems to negatively influence the RIPAS phasing procedures when more than two data sets are used.

The simultaneous use of the isomorphous and anomalous differences for estimating F_A values and locating the positions of the heavy atoms was performed by treating the RIPAS data as a MAD set. This procedure is sub-optimal and improvements need to be developed.

This work was supported in part with Federal funds from the National Cancer Institute, National Institutes of Health under contract No. NO1-CO-12400.

References

Abrahams, J. P. & Leslie, A. G. W. (1996). *Acta Cryst.* D**52**, 30–42.
Banumathi, S., Zwart, P. H., Ramagopal, U. A., Dauter, M. & Dauter, Z. (2004). *Acta Cryst.* D**60**, 1085–1093.
Brzozowski, A. M., Derewenda, U., Derewenda, Z. S., Dodson, G. G., Lowson, D. M., Turkenburg, J. P., Bjorkling, F., Huge-Jensen, B., Patkar, S. A. & Thim, L. (1991). *Nature (London)*, **351**, 491–494.
Collaborative Computational Project, Number 4 (1994). *Acta Cryst.* D**50**, 760–763.
Dall'Antonia, F., Baker, P. J. & Schneider, T. R. (2003). *Acta Cryst.* D**59**, 1987–1994.
Diederichs, K., McSweeney, S. & Ravelli, R. B. G. (2003). *Acta Cryst.* D**59**, 903–909.
Dodson, E. (2003). Private communication.
Ennifar, E., Carpentier, P., Ferrer, J.-L., Walter, P. & Dumas, P. (2002). *Acta Cryst.* D**58**, 1262–1268.
Evans, G., Polentarutti, M., Dinovic Carugo, K. & Bricogne, G. (2003). *Acta Cryst.* D**59**, 1429–1434.

Grosse-Kunstleve, R. W. & Adams, P. D. (2003). *Acta Cryst.* D**59**, 1974–1977.
Ko, T.-P., Day, J. Greenwood, A. & McPherson, A. (1994). *Acta Cryst.* D**50**, 813–825.
Kretzinger, R. H. (1968). *J. Mol. Biol.* **31**, 315–318.
La Fortelle, E. de & Bricogne, G. (1997). *Methods Enzymol.* **276**, 307–326.
Lamzin, V. S. & Wilson, K. S. (1993). *Acta Cryst.* D**49**, 129–149.
Leinala, E. K., Davies, P. L. & Jia, Z. (2002). *Acta Cryst.* D**58**, 1081–1083.
McRee, D. E. (1999). *J. Struct. Biol.* **125**, 156–165.
Morris, R. J., Zwart, P. H., Cohen, S., Fernandez, F. J., Kakaris, M., Kirillova, O., Vonrhein, C., Perrakis, A. & Lamzin, V. S. (2004). *J. Synchrotron Rad.* **11**, 56–59.
Murray, J. W., Garman, E. F. & Ravelli, R. B. G. (2004). *J. Appl. Cryst.* **37**, 513–522.
Murshudov, G., Vagin, A., Lebedev, A., Wilson, K. S. & Dodson, E. J. (1999). *Acta Cryst.* D**55**, 247–255.
Otwinowski, Z. (1991). *Proceedings of the CCP4 Study Weekend. Isomorphous Replacement and Anomalous Scattering*, edited by W. Wolf, P. R. Evans & A. G. W. Leslie, pp. 80–86. Warrington: Daresbury Laboratory.
Otwinowski, Z. (2003). Private communication.
Otwinowski, Z. & Minor, W. (1997). *Methods Enzymol.* **276**, 307–326.
Popov, A. & Bourenkov, G. (2003). *Acta Cryst.* D**59**, 1145–1153.
Ravelli, R. B. G. & McSweeney, S. M. (2000). *Structure*, **8**, 315–328.
Ravelli, R. B. G., Schrøder Leiros, H.-K., Pan, B., Caffrey, M. & McSweeney, S. (2003). *Structure*, **11**, 217–224.
Schiltz, M., Dumas, P., Ennifar, E., Flensburg, C., Paciorek, W., Vonrhein, C. & Bricogne, G. (2004). *Acta Cryst.* D**60**, 1024–1031.
Schneider, T. R. & Sheldrick, G. M. (2002). *Acta Cryst.* D**58**, 1772–1779.
Sheldrick, G. M. (2001). *XPREP* v. 6.13. Bruker-Nonius Inc., Madison, Wisconsin, USA.
Sigler, P. B. (1970). *Biochemistry*, **9**, 3609–3617.
Weiss, M. A., Mander, G., Hedderich, R., Diederichs, K., Ermler, U. & Wartenkin, E. (2004). *Acta Cryst.* D**60**, 686–695.